Opto-Electro-Mechanical Model For MOEMS

Gilles Jacquemod[1], Kimmo Vuorinen[1], Frederic Gaffiot[1], Alain Spisser[1], Christian Seassal[1],
Jean-Louis Leclercq[1], Pedro Rojo-Romeo[1], Pierre Viktorovitch[1],
Jean-Pierre Laine[2], R. Ledantec[3], T. Benyattou[3]

Abstract— **A highly selective and widely tunable optical filter based on MOEMS technology at 1.55 µm using a Fabry-Perot resonator with micromachined InP-air gap distributed Bragg reflectors has been designed and fabricated in our laboratory. The minimum resonance Full Width at Half Maximum (FWHM), as measured by micro-reflectivity experiments, is close to 0.4 nm (around 1.55 µm) and the continuous tuning range is around 60 nm for a bias voltage of 14 V.**
In order to study the global characteristics of this device, an opto-electro-mechanical behavioral model has been developed. The model, written in VHDL-AMS-like Hardware Description Language, allows a combined simulation of optical, electrical and mechanical behavior of the tunable optical filter in a mixed-signal electronics design framework. Moreover, the use of Hardware Description Language allows an integration of the model in a system simulation context.

Index terms-- **MOEMS, optical filter, Hardware Description Languages, behavioral modeling, WDM**

I. Introduction

WDM system technology using a new generation of smart micromachined optoelectronic devices appears most promising for a wide range of communication applications such as optical networks, fibre-to-the-house systems, computer interconnections, multi-media systems [1-3]. Among the most essential devices that are needed around 1.55 µm, monolithic highly selective and tunable optical filters based on InP micro-opto-electro-mechanical systems (MOEMS) are very promising [4-6]. The key performances of optical filters requested by WDM systems for telecommunication applications are (i) a high wavelength selectivity, enabling the selection of neighbouring channels 1.6 nm apart with a crosstalk ratio of 20 dB, (ii) a continuous wavelength tuning range of about 30 nm around 1.55 µm (compatible with the bandwidth of Erbium Doped Fiber Amplifier), with no degradation of the selectivity.

Ecole Centrale de Lyon
[1] LEAME - UMR CNRS 5512
[2] LTDS - UMR CNRS 5513
BP 163, F-69131 Ecully Cedex, France
[3] INSA de Lyon, LPM - UMR CNRS 5511
F-69621, Villeurbanne Cedex, France

In order to optimize the global characteristics of the tunable optical filter, integrated simulation of optical, electrical and mechanical behavior is necessary. This approach, already used for MEMS modeling, allows a simulation of a complete system using electrical and non-electrical components. For example, SPICE-like models for MEMS have been developed by using equivalent circuits [7-9] or an additional program, which translates the mechanical equations to Spice-netlists [10]. An other approach consists of using mixed-signal Hardware Description Language, like VHDL-AMS, in microsystem modeling [11-13]. This method is well suited for complete system modeling, since it supports hierarchical system description and allows to integrate digital, analog and non-electrical functions in the same simulation framework [14]. The hierarchical nature of the language provides a natural way to reduce the gap between system and circuit design. Moreover, it can be used even in larger system design context, such as hardware software co-design [15].
This paper presents the design and the fabrication of a vertical micromachined InP-air gap based Fabry-Perot filter, continuously tunable via electrostatic actuation of the cavity air gap. A behavioral model of this device, written using VHDL-AMS-like Hardware Description Language, HDL-A™ [11], has been developed. The simulated results are compared with experimental data. Finally, the behavioral model is used in transmission layer simulations of a WDM optical communication network.

II. MOEMS design

The filters comprise of a Fabry-Perot air gap resonant cavity formed between two high reflectance Bragg mirrors based on InP/air-gap pairs. Due to the high index contrast between the air and the InP quarter-wave layers, reflectivity as high as 99.9 % is achieved with only 2.5 pairs (Fig. 1). All reflector and cavity air gaps can be easily fabricated by selective micromachining of InGaAs sacrificial layers [16]. The top mirror is p-doped, the cavity is non-intentionally doped and the bottom mirror is n-doped to form a p-i-n junction, which can be reversely biased. The electrostatic tuning voltage is applied to the layers adjacent to the Fabry-Perot cavity, thus reducing its thickness and tuning the resonant wavelength.

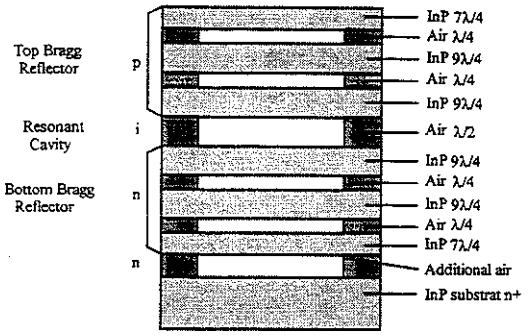

Figure 1. Schematic view micrograph of the micromachined filter structure.

The structure was grown by LP-MOCVD (Low Pressure-Metallo Organic Chemical Vapour Deposition) lattice matched to InP (001) substrate. AuGe and Pd/AuGe alloys were formed respectively for the back and top ohmic electrostatic tuning contacts of the filter. Surface micromachining technology is used to fabricate the filter : it implies a first step of non selective vertical patterning by Reactive Ion Etching (RIE) with CH_4:H_2 ; in a second step, the suspended layers are freed by selective lateral wet underetching of the InGaAs sacrificial layers with HF:H_2O_2:H_2O solution. The sample is successively rinsed in H_2O and methanol (x3), and dried with a supercritical carbon dioxide drying technique recently developed in our laboratory. Smooth optical graded non-sticking multi air gap InP paddle-shaped bridges were fabricated (Fig. 2) : the central (30x30 μm^2) platforms are suspended by two, 5 μm wide and 30 μm length, arms.

Figure 2. SEM micrograph of a paddle-shaped bridge.

A previous version of this filter has been realized without platforms, the bridges are only made by clamped-clamped 20 μm wide and 50 μm up to 250 μm long beams [17].

III. Modeling of the MOEMS using HDL-A

A. Simulation environment

A mixed-signal simulation environment is used to model and simulate the MOEMS. It consists of a mixed-signal simulator with user-defined HDL-A™-/C-language model entries and a build-in SPICE-like/macromodel library. The HLD-A™/C-interface allows user-defined models to be compiled and integrated with circuit-level models into the simulator (Fig. 3). Although HDL-A™/C is primarily dedicated to mixed-signal electronics system modeling, non-electronic system models are also supported.

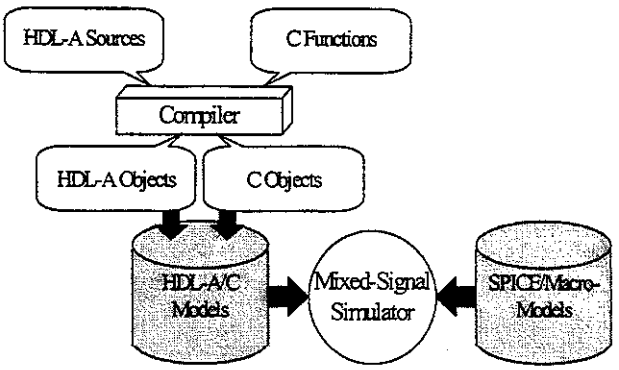

Figure 3. Modeling and simulation environment.

The HDL-A™ models contain two main parts: entity and architecture. The entity is the external view of the model with parameters, analog and digital connections. One or several architectures can be used to describe the analog, digital or mixed analog and digital behavior of the model. The semantics and syntax of HDL-A™ are based on VHDL. The analog behavior can be modeled using explicit or implicit algebraic and differential equations in dc, ac or transient domains. The process block, describing digital behavior of the model, is similar to VHDL. C-function calls are also allowed from both analog and digital parts of the model. The simulation environment allows to simulate individual components as well as system or subsystem.

B. Modeling of the MOEMS

The behavioral model of the optical tunable filter is shown in figure 4. Electrically, it behaves like a reversed biased pin diode. The tuning voltage induces an electrostatic force to the layers adjacent to the cavity, thus reducing its thickness and the resonant wavelength.

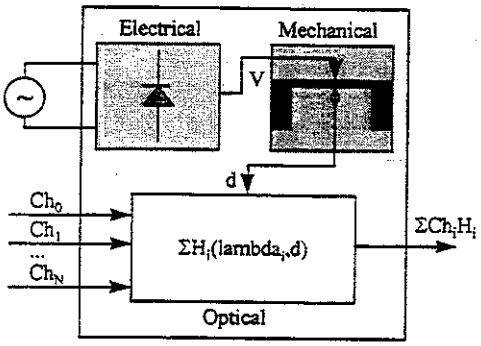

Figure 4. Opto-electro-mechanical behavioral model.

The electrical behavior of the MOEMS depends on the physical and geometrical parameters of the bridge. The figure 5 gives the top view of a bridge. The electrical equivalent circuit of this device is given in figure 6, the series resistance R_S is related to ohmic contacts.

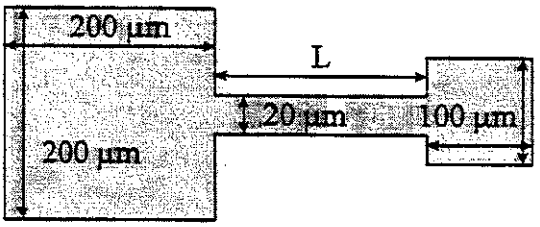

Figure 5. Top view of a beam.

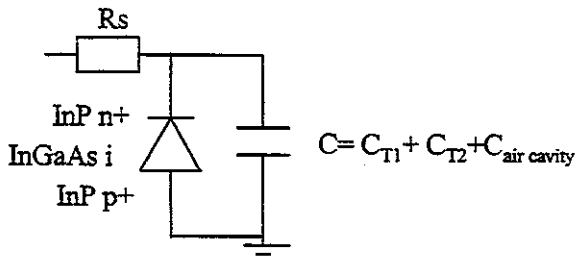

Figure 6. Equivalent circuit model of the MOEMS.

The transition capacitance of a reverse-biased pin diode is equivalent of a parallel-plate capacitor [18] :

$$C_T = \varepsilon \frac{S}{w} \qquad (3.1)$$

where S is the junction area (200x200 µm² for C_{T1} and 100x100 µm² for C_{T2}), ε is the permittivity of the semiconductor (ε_r = 12.1 for InP).
Considering that $w=w_0=\lambda/2=0.775\mu m$ (λ=1.55µm), the capacitance C_T is given by :

C_{T1} = 5.5 pF and C_{T2} = 1.4 pF
$C_T = C_{T1} + C_{T2}$ = 6.9 pF

The cavity capacitance can be also calculated by using 3.1, where ε is the permittivity of air, S the beam area (S = bxL, b=20 µm). For a 200 µm beam length, the cavity thickness is at zero bias $w=w_0=0.775\mu m$ and $C_{air\ cavity}$ = 0.05 pF. If we consider the beam motion as an horizontal displacement (neglecting the beam curvature) with a 255 nm maximum displacement, the maximum cavity capacitance is increased to 0.07 pF. Since $C_{air\ cavity} << C_T$, the cavity capacitance is not taken into account in the behavioral model.

The diode voltage V_D drives directly the beams, responsible of filter tuning. The clamped-clamped beam has several mechanical resonance modes. However, by considering only the first mode, this gives a good approximation of the bending (error < 2%). Thus, the dynamics of the beam is described by a second order motion equation [7] :

$$M\frac{d^2x}{dt^2} + \gamma\frac{dx}{dt} + kx = \varepsilon\frac{SV_D^2}{2w^2} \qquad (3.2)$$

where t is time, x is the displacement, M the mass and S the area of the beam, γ is the damping coefficient and k the spring constant. The electrostatic interactions are related to the cavity thickness w= w_0-2x, where $w_0=\lambda/2=0.775\mu m$.
The spring constant is given by :

$$k = M(2\pi f_0)^2 \qquad (3.3)$$

The first mode is the normal bending mode with resonance frequency determined by :

$$f_0 = \frac{A^2}{2\pi L^2}\sqrt{\frac{EI}{M}} \quad \text{with } I = \frac{bh^3}{12} \qquad (3.4)$$

where E is the modulus of elasticity, A the modal constant. I is the area moment of inertia of beam about neutral axis, and h the thickness of the beam.

The optical behavior of MOEMS is determined by transfer matrix method [19]. The global transfer matrix [T] of a MOEMS, including N successive layers, is a product of N transfer matrices $[T_i]$, taking into account the interface i,i+1, the thickness d_i and the wave vector k_i of each individual layer (see relation 3.5).

$$[T] = \begin{pmatrix} T_{11} & T_{12} \\ T_{21} & T_{22} \end{pmatrix} = [T_1][T_2]...[T_N] \qquad (3.5)$$

T_{ij} are known as the transmission coefficients of the structure. Each transfer matrix is given by :

$$[T_i] = [P_i]\,[I_{i,i+1}] \text{ , with}$$

$$[P_i] = \begin{pmatrix} e^{-jk_id_i} & 0 \\ 0 & e^{+jk_id_i} \end{pmatrix}$$

$$[I_{i,i+1}] = \begin{pmatrix} \frac{\eta_i + \eta_{i+1}}{2\eta_i} & \frac{\eta_i - \eta_{i+1}}{2\eta_i} \\ \frac{\eta_i - \eta_{i+1}}{2\eta_i} & \frac{\eta_i + \eta_{i+1}}{2\eta_i} \end{pmatrix}$$

$$\text{with } \eta_i = \sqrt{\frac{\mu_i}{\varepsilon_i}} \qquad (3.6)$$

When a time domain simulation of the entire component including electrical, mechanical and optical behavior is required, modifications of the thickness of the air cavity as well as the two air gaps next to the cavity, due to applied electrostatic force, are updated to the global transfer matrix [T] at each simulator time step. We have assumed that the information channel bandwidth B_I is small compared to the optical filter bandwidth B_F. Thus, the optical output O of the model is a sum of the contributions of each individual channels, calculated by multiplying the channel contents $ch_i(\lambda_i,t)$ by its transfer function $H_i\{[T(\lambda_i,x(t))]\}$ at λ_i, where x(t) is the displacement of the beam center :

$$O = \sum_i H_i\left\{\left[T(\lambda_i, x(t))\right]\right\} ch_i(\lambda_i, t) \qquad (3.7)$$

If condition ($B_I << B_F$) is not valid, Z-transform has to be used in order to calculate the filter response in time domain.

IV. Simulation Results

A. *Model validation*

The MOEMS were characterized with a micro-reflectivity experimental set-up (spot size of 2.5 x 50 μm^2). The experimental spectrum of the unbiased filter shows a Full Width at Half Maximum (FWHM) of 0.8 nm. Figure 7 gives the comparison between the experimental and the simulated results of the first MOEMS.

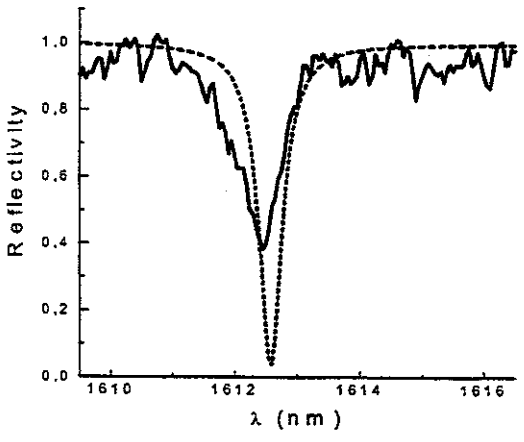

Figure 7. Experimental and simulated results.

The filter tuning spectra of the second MOEMS are shown in figure 8. Tuning was achieved over a wavelength range of 70 nm for an applied voltage of 14 V across the cavity air gap. The filter F.W.H.M. is kept below 1 nm over a tuning range of 40 nm. Then, it starts to increase probably due to the combined effects of the electrostatic deformation of the suspended beams and of the shift of the resonance peak close to the high energy boundary of the Bragg reflector stop band.

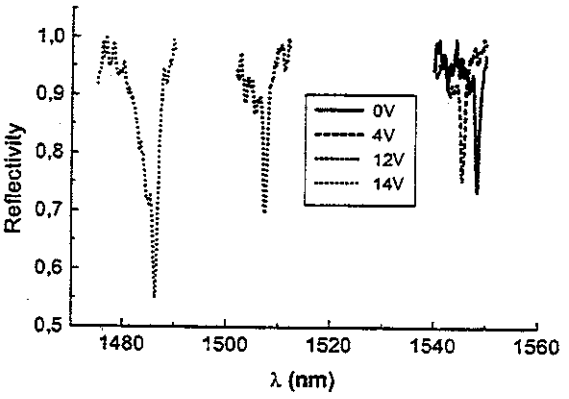

Figure 8. Experimental tuning spectra of the second filter.

Simulated tuning spectra of the second MOEMS are shown in figure 9. The spring constant (relation 3.2) and the optical thickness are adjusted to fit experimental spectra.

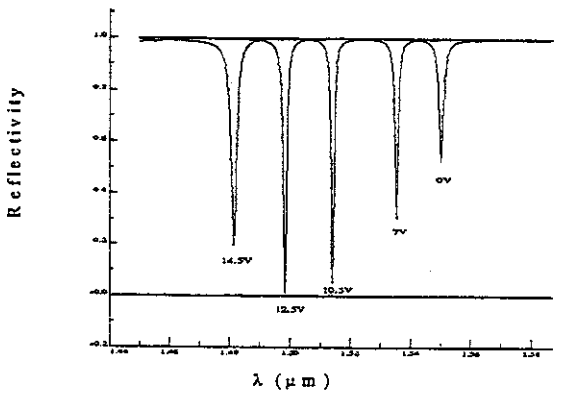

Figure 9. Simulated tuning spectra.

Non-uniformity of the minimum reflectivity value is due to bending of the upper beam. Nevertheless, comparing both spectra, we notice discrepancy in reflectivity values. With a such suspended multi-layers structure, stochastic bending of inner beams can also occur and cannot be easily taken into account in the model. However, the simple fitting procedure used here describes well the resonance wavelength shift as shown in figure 10.

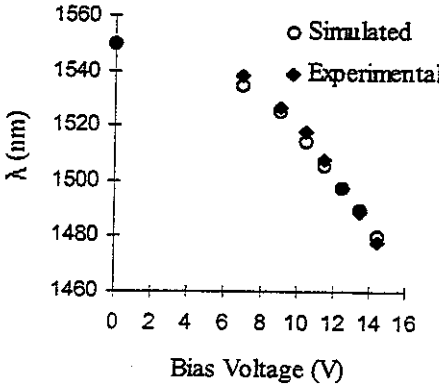

Figure 10. Comparison between experimental and simulated tuning characteristics.

The resonance wavelength shift does not fit a square law as expected due to electrostatic interactions (Fig. 11). The mechanical displacement (relation 3.2) is modeled, on one hand, with a constant value of w (case a : $w=w_o$), and on the other hand, with a variable value of w (case b : $w=w_o-2x$).

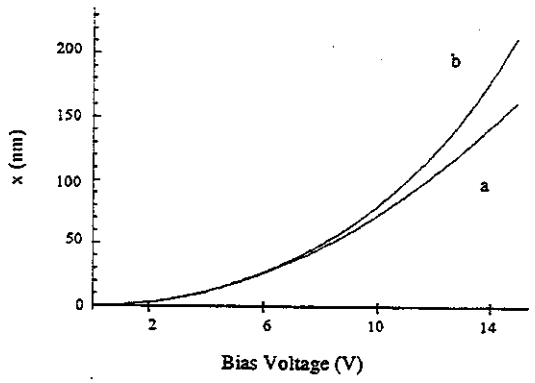

Figure 11. Displacement of the beam center : (a) without and (b) with electrostatic interactions.

Optical and opto-electro-mechanical characterizations have been made in DC domain, and show a good agreement with the simulated results. The mechanical displacement is more important than the resonant wavelength shift. This is due to the fact that the resonant wavelength shift does not only depend on the air cavity thickness, but is also related to the optical structure of the device. In fact, the electromagnetic field is not perfectly confined in the air cavity, but also extends in the Bragg mirrors.

B. *Dynamic simulation*

Tuning delay, like tuning range and selectivity, is very crucial design parameter for the tunable optical filter in packet switched WDM network applications. The physical design parameters of the MOEMS, especially the device geometry has a strong influence on tuning delay. This is illustrated in figure 12 and 13, showing the resonance frequency (f_o, relation 3.4) and the tuning delay ($T_d=1/3\ f_o$) respectively. We have assumed that the dynamic response of the device is inertia dominated. This allows to determine the lower limit of the tuning delay for the MOEMS, by using an optimal multi-step command [20]. In practice, tuning delay is also limited by air damping.

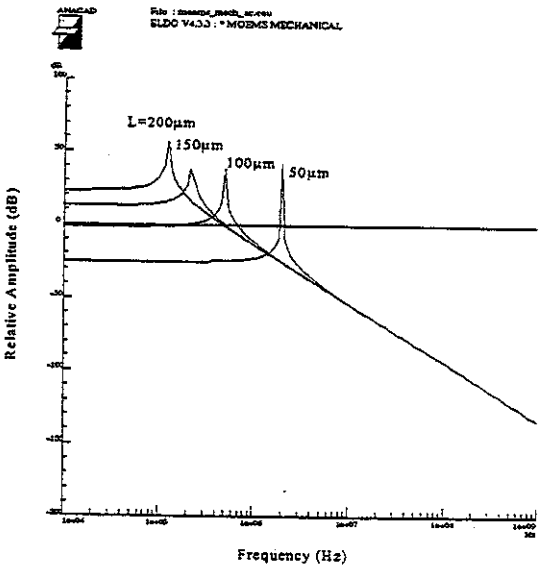

Figure 12. Frequency response of the device for different beam lengths.

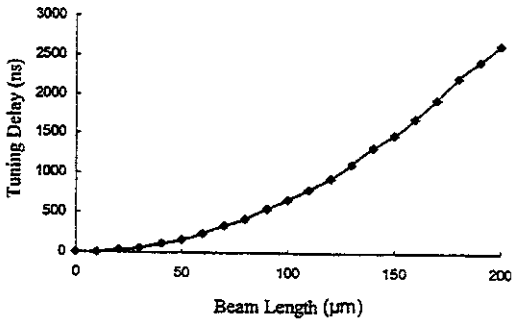

Figure 13. Tuning delay for an optimal multi-step command.

C. *Behavioral system simulation*

The behavioral model of the tunable optical filter can be integrated with photonic and electronic components, as well as the software in a unique simulator (ELDO™) in order to co-simulate the control and data path of a WDM optical communication network. The simulated network consists of four nodes, each having one transmitter and two MOEMS-based tunable optical filters in the receiver branch [21]. The cross-talk penalty (without phase noise, Fig. 14), extracted

from transmission layer simulation of the network [21], is estimated from simulated eye diagrams as follows :

$$P_c(dB) = 10\log\left(\frac{E_I}{E_c}\right) \qquad (4.1)$$

where E_i is the maximum vertical eye opening when all the neighboring channels are inactive and E_C the eye opening when all the channel are active.

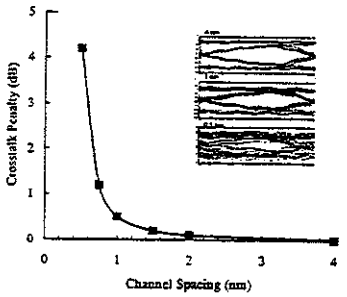

Figure 14. Simulated cross-talk penalty (Optical filter bandwidth : 0.5 nm) .

V. CONCLUSIONS

An analytical behavioral model for micro-opto-electro-mechanical tunable optical filter has been developed. The model can be used, in one hand for design optimization, and in the other hand for evaluation of measured or extracted parameters on the global electro-opto-mechanical response of the device. The measured characteristics of the sample device are well described by the simple behavioral model. However, for an accurate component simulation, the model parameters have to fit to experimental values. This can be very difficult due to the stochastic nature of many device parameters, so the use of table-based modeling might be more appropriate [11]. Moreover, the use of Hardware Description Language, like VHDL-AMS, allows (i) hierarchical description, (ii) integration of the device in a system simulation, (iii) simulator independency.

References

1. M.Y. Li, W. Yuen and C.J. Chang-Hasnain, "Wide and continuously tunable (30 nm) detector with uniform characteristics over tuning range", *Electron. Lett.*, vol. 33, n° 13, June 1997, pp. 1122-1124
2. M.C. Larson, A.R. Massengale and J.S. Harris, "Continuously tunable micomachined vertical cavity surface emitting laser with 18 nm wavelength range", *Electron. Lett.*, vol. 32, No. 4, Feb. 1996, pp. 330-332
3. M. S. Wu, G. S. Li, W. Yuen and C.J. Chang-Hasnain: "Widely tunable 1.5 µm micromechanical optical filter using AlO_x/AlGaAs DBR", *Electron. Lett.*, vol. 33, n° 20, Sep. 1997, pp. 1702-1704
4. K. Streubel, S. Rapp, J. André and N. Chitica: "1,26 µm vertical cavity laser with two InP/air-gap reflectors", *Electron. Lett.*, vol. 32, n°15, July 1996, pp. 1369-1370
5. K. Hjort, et al.: "Demands and solutions for an indium phosphide based micromechanically tunable WDM photodetector", *MOEMS 97 International conf. on optical MEMS and their applications*, Nara (Japan), Nov. 1997
6. C. Seassal, et al., "InP-based micro-mechanical and selective photodetector for WDM systems", *Proc. SPIE Miniaturized Systems with Micro-Optics and Micromechanics II*, Feb. 1997, vol. 3008, pp. 62-67
7. T. Veijola, H. Kuisma, J. Lahdenpera and T. Ryhanen, "Equivalent-circuit model of the squeezed gas film in a silicon accelerometer", *Sensors and Actuators A 48*, 1995, pp. 239-248
8. R.K. Gupta, E.S. Hung, Y.J. Yang, G.K. Ananthasuresh and S.D. Senturia, "Pull-in dynamics of electrostatically-actuated beams", *Proc. Solid-state Sensor & Actuator Workshop*, June 1996
9. G.K. Ananthasuresh, R.K. Gupta and S.D. Senturia, "An approach to macromodeling of MEMS for nonlinear dynamic simulation", *ASME 96 Interntional Mechanical Engineering Congress and Exposition, Proc. Of Dynamics Systems and Controls*, DSC-vol. 59, Atlanta, Nov. 1996, pp. 401-407
10. G. Pelz, J. Bielefeld, F.J. Zappe and G. Zimmer, "Simulating micro-electromechanical systems", *IEEE Circuits and Devices Magazine: Simulation and Modeling*, Ed. R. Saleh and A. Yang, March 1995, pp. 10-13
11. A. Vachoux, J.M. Bergé, O. Levia and J. Raillard, "Analog and Mixed-Signal Hardware Description Languages", *CIEM 10, Kluwer Academic Publishers*, 1997
12. A. Boegli, V. Moser, H. P. Amann, F. Pellandini, B. Romanowicz, Ph. Lerch, M. Laudon, Ph. Renaud, "System-Level Simulation Using Mixed-Nature Models", *1st Europe-Asia Congress on Mechatronics*, Besancon, (France), Oct. 1996, pp 12 - 17.
13. B. Romanowicz, Y. Ansel, M. Laudon, C. Annacker, Ph. Renaud, A. Vachoux, and G. Schröfer, "Modeling and simulation of microsystems - An experience with HDL-A", *Workshop on libraries, component modeling and quality assurance*, IRESTE-IHT, Nantes, Apr. 1995
14. K. Vuorinen, F. Gaffiot, and G. Jacquemod, "Modeling single-mode lasers and standard single-mode fibers using a Hardware Description Language", *IEEE Photon. Technol. Lett.*, vol. 9, no. 6, 1997, pp. 824-826,
15. M. Knieser and C. Papachristou, "COMET: a hardware-software codesign methodology", *Proc. EURO-DAC'96*, 1996
16. C. Seassal, J.L. Leclercq and P. Viktorovitch, "Fabrication of InP-based freestanding microstructures by selective surface micromachining", *J. Micromech. Microeng.*, vol. 6, 1996, pp. 261-265
17. A. Spisser, et al.: "Highly selective 1.55 µm InP/air-gap micromachined Fabry-Perot filter for optical communications", *Electron. Lett.*, vol. 34, n° 5, 1998, pp. 453-455
18. J. Millman and C.C. Halkias, "Integrated electronics : analog and digital circuits and systems", Mc Graw-Hill Tokyo, 1986
19. S. Ramo, J.R. Whinnery, and T. van Duzer, "Fields and Waves in Communication Electronics", *John Wiley & Sons, Singapore*, 1984, pp. 535-547
20. K. Hogari and T. Matsumoto, "Electrostatically driven fiber-optic micromechanical on/off switch and its application to subscriber transmission systems", *J. Lightwave Technol.*, vol. 8, n° 5, May 1990, pp. 722-727
21. K. Vuorinen, G. Jacquemod, F. Gaffiot & C. Seassal, «A behavioral modeling approach for optical communication network design», SPIE, vol. 3290, Proc. Optoelectronic Integrated Circuits II, San Jose, 1998, p. 353-363